Permanent-Magnet System Field Distribution on the Surface of Smooth FER Romagnetic Core

Vasiliy Germanovich Chirkin[1], Vladimir Ivanovich Goncharov[1], Sergey Vladimirovich Shirinskii[1], Lev Yurievich Lezhnev[2] and Dmitry Anatolyevich Petrichenko[2]

[1]National Research University "Moscow Power Engineering Institute" 111250, Russia, Moscow, Krasnokazarmennayastr, 14.
[2]Moscow State University of Mechanical Engineering (MAMI) 107023, Russia, Moscow, B. Semenovskaya str., 38.

The known analytical solution of the field problem considering magnetic field of a thin linear conductor placed above smooth ferromagnetic core have been used to analyze the normal component of the flux density distribution created by a system of permanent magnets on the surface of a core. Ampere model of a permanent magnet initially have been used with the assumption of lack of other ferromagnetic objects. Then a number of numerical experiments have been carried out to take into account ferromagnetic elements in the vicinity of the permanent magnets and graphical dependences of the flux density and magnet sizing were obtained.

Key words: Electric machine; Permanent magnet; Analytical expression; Finite-element modeling; Magnet sizing.

When designing linear electric machines, both generators and motors, the problem arises of the reasonable relations between dimensions and electromagnetic loads, in particular between the pole pitch and air-gap flux density. Such a problem arises usually at the initial stage of a design and it is very desirable to use analytical expressions in this case.

In recent years, numerous papers concerning air-gap field of permanent magnet (PM) electric machines (PMEMs) have been published. For example, in (Amara & Barakat, 2010), the magnetic field under load operating condition is considered as superposition of the no-load field produced by PMs and the armature winding field.

The analytical solutions of the field problems stated forthe smooth air gaps were used. The slotting was allowed by using the proper air-gap coefficients. The method proposed was recommended for designing of tubular linear machines.

The lot of papers based on analytical approach were devoted to the teeth-conditional electromagnetic torque pulsations, called cogging torques, which are specific to PMEMs and must be minimized (Zarko, Ban, & Lipo, 2008), (Chu & Zhu, 2013). Thus in (Zarko, Ban, & Lipo, 2008) cogging torques were determined integrating Maxwell stresses along the air gap contour. Radial and tangential components of the air-gap flux density distribution were found using the conformal mapping that allowed for the stator slotting. For the four-pole 7 kW motor with surface-mounted magnets (SPM), the analytical calculation results were in good agreement with the finite-element analysis.

---

* To whom all correspondence should be addressed.

To determine the torque pulsation under load operating condition is the more complicated problem than determining the no-load cogging torques. In (Chu & Zhu, 2013) the authors make up a conclusion that though the lot of works dealt with this problem (the paper's bibliography includes 39 references) there are no satisfactory methods to calculate the under-load torque pulsation so far. The authors propose new method based on virtual work conception and using the frozen relative magnetic permeability distribution. The results of finite-element modeling confirm the proposed method accuracy.

Several papers concerning analysis of the air-gap field in PMEMs (both rotating and linear machines) were published by the research group head by E.A. Lomonova: (Overboom, Smeets, Jansen, & Lomonova, Semianalytical calculation of the torque in a linear permanent-magnet motor with finite yoke length., 2012), (Overboom, Smeets, Jansen, & Lomonova, Topology comparision for a magnetically suspended ceiling actuator., 2011), (Krop, Lomonova, & Vandenpit, 2008), (Gysen, Meesen, Paulides, & Lomonova, 2010). In the first paper listed above, for instance, analytical expressions allowing for the core slotting and longitudinal end effect were used for determining the propulsion and normal forces in linear PM motor. The forces were calculated integrating the Maxwell stresses along the contour tightly closed to the core surface. The results were used to estimate the bearings operating conditions in the reliability estimation.

Analytical methods were used also for analysis of the fields in the PMEMs with magnetic reduction of the speed including the air-gap and tooth-tip leakage. In particular, in (Li, Chau, Liu, Gao, & Wu, 2013) leakage parameters were determined for the low-speed linear motors for which this problem is very important. Accuracy of the analytical expressions derived in that paper was confirmed by the FEM analysis.

It is very important for high-speed PMEMs to determine accurately the PM losses. An example of such works as (Wu, Zhu, Staton, Popesku, & Hawkins, 2012) where the analytical procedure was developed for predicting the open-circuit magnet eddy-current loss due to slotting. The developed model is capable of providing both high accuracy and insights of loss generation. The

influence of such factors as slot opening to slot-pitch ratio, slot and pole number combination, pole-arc to pole-pitch ratio were investigated. The finite-element results validate high accuracy of the developed analytical model.

Analytical solution of the field produced by Halbach-array PM-system was presented in (Hoburg, 2004). The assumptions made were, first, that the PM array was very long and, secondly, that only the fundamental field harmonic is considered, which decays in normal direction more slowly than high-order harmonics. It was shown that the accuracy of the model developed was sufficiently good for large dimension machines, such as linear motors for high-speed ground transportation.

The purpose of this paper is to present an analytical modeling approach for analyzing the on-surface distribution of the magnetic field produced by PM-systems on the flat ferromagnetic core
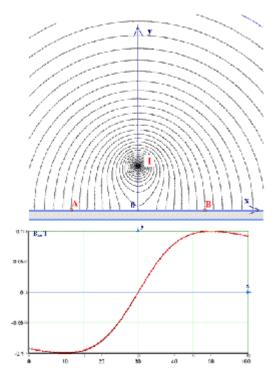

Fig. 1. Magnetic field pattern for the case of thin current-carrying conductor located above the flat ferromagnetic core and plots of the normal flux-density component determined on the *AB* part of the core. Both analytical (calculated by (4)) and *FEM*-modeling results are presented (both plots practically coincide).

Problem formulation and solution

At the beginning, let us consider the flux-density normal component of the plane magnetic field produced by the PM-system located above the flat ferromagnetic core assuming that there no other soft-magnetic bodies.

It is known (Ivanov-Smolenskii & Abramkin, Application of conformal mapping for electromagnetic analysis of electric machines: Analytical methods (in Russian), 1970), (Ivanov-Smolenskii & Abramkin, Application of conformal mapping for electromagnetic analysis of electric machines (in Russian), 1980) an expression for the complex potential $w(z) = \varphi + j\psi$, where φ is the magnetic field intensity flux function, which is stated using a magnetic vector potential $\varphi = \dot{A}_z/\mu$ (μ is a medium magnetic permeability), and y is the scalar magnetic potential, for the field created by a thin linear current placed on the ordinate axis above the soft-magnetic core (fig. 1):

$$w(z) = (I/2\pi)\ln(z^2 + g^2) \qquad ...(1)$$

where g is the height of the conductor.

Locating real axis $0x$ along the core surface we will obtain

$$w(z) = \varphi(x) = (I/2\pi)\ln(x^2 + g^2) = (1/\mu)\dot{A}_z \qquad ...(2)$$

Taking into account that normal component of the flux-density on-surface distribution can be expressed as

$$B(x) \cdot dx = \mu_0 \frac{I}{2\pi}\left(\ln(x^2 + g^2)\right) \qquad ...(3)$$

we will obtain

$$B(x) = \mu_0 \frac{I}{2\pi} \frac{2x}{x^2 + g^2} \qquad ...(4)$$

Expression (4) makesit possible to deduce the formula for distribution of the normal flux density of the magnetic field produced by a single PM placed above the flat core. In order to do this let us present the PM by its Ampere model, i.e. by two thin current layers with constant linear current density equal *modulo* to the PM coercive intensity.

For the current layer with linear current density j_z located above the core (fig. 2) one can write based on (4):

$$dB(x) = j_z db_m \cdot \frac{\mu_0}{\pi} \cdot \frac{x}{x^2 + g^2} \qquad ...(5)$$

and

$$B(x) = \frac{\mu_0}{\pi} \cdot j_z \cdot \int_{b_{mx} - b_m/2}^{b_{mx} - b_m/2} \frac{x + b_{mx}}{(x + b_{mx})^2 + g^2} db_m. \qquad ...(6)$$

Integrating (6) we obtain:

$$B(x) = \frac{\mu_0}{2\pi} \cdot j_z \cdot \ln\left[\frac{(x + 0{,}5b_m)^2 + g^2}{(x - 0{,}5b_m)^2 + g^2}\right] \qquad ...(7)$$

Ampere model of the PM magnetized along the real axis x looks like two current layers with oppositely directed current densities placed one above other at a distance h_m. In this case, the
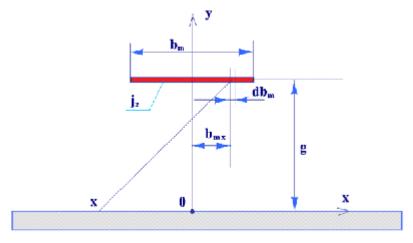

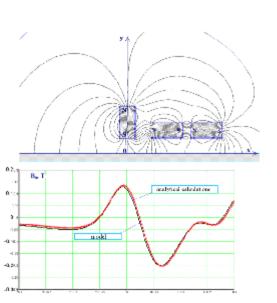**Fig. 2.** Current layer with linear current density j_z located above the core

distribution of the flux-density normal component can be described by the following expression:

$$B(x) = \frac{\mu_0}{2\pi}(-1) \cdot j_* \cdot \ln\left\{\frac{\left[(x+0.5b_*)^2+g^2\right] \cdot \left[(x-0.5b_*)^2+(g+h_*)^2\right]}{\left[(x-0.5b_*)^2+g^2\right] \cdot \left[(x+0.5b_*)^2+(g+h_*)^2\right]}\right\} \quad ...(8)$$

Distribution of the flux-density normal component along the core surface for the *k-th* magnet shifted from the Y-line at the distance Δx_k can be derived from (8):

$$B_k(x) = \frac{\mu_0}{2\pi}(-1) \cdot j_{zk} \cdot \ln\left\{\frac{\left[(x-\Delta x_k+0.5b_{mk})^2+g_k^2\right] \cdot \left[(x-\Delta x_k-0.5b_{mk})^2+(g_k+h_{mk})^2\right]}{\left[(x-\Delta x_k-0.5b_{mk})^2+g_k^2\right] \cdot \left[(x-\Delta x_k+0.5b_{mk})^2+(g_k+h_{mk})^2\right]}\right\} \quad ...(9)$$

While deriving (8) and (9), it was supposed that the upper layers current density is positive and of the lower ones is negative. If the PM is magnetized in the direction opposite to that of the real axis signs of the current densities must be changed.

The flux-density normal component of the field produced by the system of PMs manufactured from the same material and magnetized in directions parallel to the real axis can be written as follows:

$$B_{zn}(x) = \frac{\mu_0}{2\pi}(-1)j_z \sum_{k=1}^{K} \ln\left(\frac{A_z1 \cdot A_z2}{A_z3 \cdot A_z4}\right) \quad ...(10)$$

$$A_z1 = (x - \Delta x_k + 0.5b_{mk})^2 + g_k^2 \quad ...(11)$$

$$A_z2 = (x - \Delta x_k - 0.5b_{mk})^2 + (g_k + h_{mk})^2 \quad ...(12)$$

$$A_z3 = (x - \Delta x_k - 0.5b_{mk})^2 + g_k^2 \quad ...(13)$$

$$A_z4 = (x - \Delta x_k + 0.5b_{mk})^2 + (g_k + h_{mk})^2 \quad ...(14)$$

In (11)-(14) b_{mk} denotes the dimension of the *k*-th magnet along the *x*-axis, and h_{mk} along the *y*-axis.

In the similar way, with only difference that integration must be performed along the *y*-axis, the expressions can be derived for the normal flux-density distribution for the PM magnetized in vertical direction. Deriving such expressions for the PM symmetrically positioned with respect to the *y*-axis and taking into account intervals between magnets in *x*-direction then one can obtain
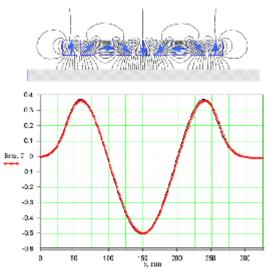

Fig. 3. The normal component of flux-density distribution of the field produced by the PM-system on the surface of flat core

Fig. 4. Flux-lines pattern and on-core-surface normal flux-density distributions of the field produced by *Halbach* PM-system

for the system of vertically magnetized PMs the following:

$$B_{yn}(x) = \frac{\mu_0}{\pi} j_z \left(A_y 1 - A_y 2 - A_y 3 + A_y 4 \right)$$

...(15)

$$A_y 1 = arctg \left(\frac{g + h_m}{x + 0.5 b_m} \right) \qquad ...(16)$$

$$A_y 2 = arctg \left(\frac{g}{x + 0.5 b_m} \right) \qquad ...(17)$$

$$A_y 3 = arctg \left(\frac{g + h_m}{x - 0.5 b_m} \right) \qquad ...(18)$$

$$A_y 4 = arctg \left(\frac{g}{x - 0.5 b_m} \right) \qquad ...(19)$$

As an example, fig. 3 illustrates the normal flux density distributions of the PM-system calculated using the above analytical expressions and obtained on the *FEM* models (both plots practically coincide)

The use of Ampere models makes it possible to determine the flux-density distributions not only for magnets magnetized along the co-ordinate axes but also for PMs magnetized in whatever directions. In this case the PM must be represented by four, not two, current layers, the linear current density of the layers representing the *x*-magnetization (*x*-layers) being the coercive intensity multiplied by the cosine of the angle between the magnetization and *x*-axis directions, and of the *y*-layers by the sine of this angle. In fig. 4, the field lines pattern and on-surface flux-density distributions of *Halbach*-array PM-system. Both analytical and *FEM*-modeling results are very close.

The use of expressions derived allows finding optimal relations between the characteristic dimensions of the magnetic systems of PMEMs in cases when certain restrictions set, for example,
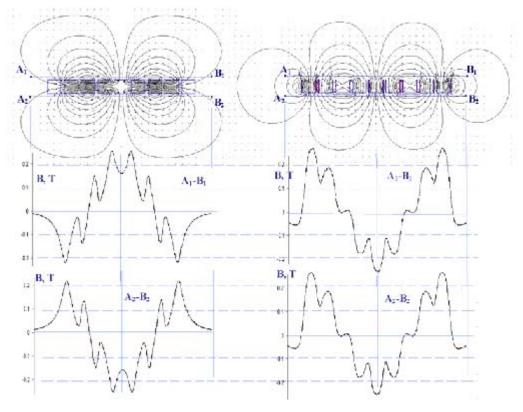

Fig. 5. Magnetic fields and flux-density normal component distributions along the straight contours above and underneath Halbach array. Magnetic field patterns and plots are obtained using the FEM-models of x- and y-current layers of PM Ampere-models.

on the volume, on the air-gap length or on minimal value of the air-gap flux density.

Using Ampere models enable to demonstrate and explain the peculiarity of Halbach magnetic field. Let us perform following experiment on FEM-model. Let us form the Halbach PM-system (often called Halbach array) consisting of nine PMs in the form of bars with square cross-section 20×20 mm^2 and located in expanded range at a distance 25 mm one from another. Suppose that bars are long enough to consider magnetic field as plane. Let us draw two contours $\grave{A}_1 B_1$ and $\grave{A}_2 B_2$ above and underneath the magnets to "measure" normal components of flux density (Fig. 5).

This feature of the Halbach assembly magnetic field can be used in machines with permanent magnets on the rotor (in the case of

rotating machines) or on the moving part (inductor) of linear machines to make it lighter by avoiding massive ferromagnetic yokes. For example, (Jang, You, Ko, & Choi, 2008) describes a model of a 30 kW 20 000 rpm synchronous machine for flywheel energy storage, with a double-sided rotor. The both sides of rotor, i.e the outer and inner part, are magnetized by permanent magnets arranged as Halbach assembly. The authors calculated the no-load mode and obtained the time dependence of the armature winding back-emf. Some details of the project: the diameter of the outer rotor is 208 mm, active length is 50 mm, litz-wire winding, current of 64 A at a current density of 5 A/mm^2, the permanent magnets residual flux density - 1.23 Tesla. The test results produced on a prototype are in good agreement with the calculation.
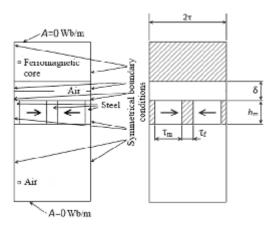

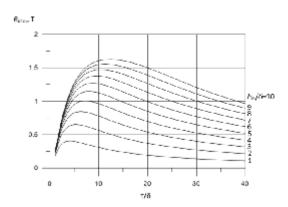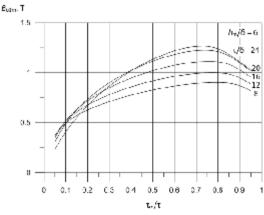**Fig. 6.** The finite-element model, materials and boundary conditions

Fig. 7. Plots of the amplitude of the first harmonic of the magnetic flux density at $\alpha = 1$ mm and $h_m/\varphi = 6$ as a function of τ_m/τ

Fig. 8. First harmonic amplitude of the flux density vs τ/α for different h_μ/α (at $\alpha = 1$)
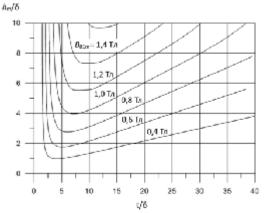

Fig. 9. The permanent magnets relative height vs relative length of the pole pitch $h_m/\alpha = f(\tau/\alpha)$ for $B_{\alpha 1m} = const$

Suppose that magnetization vector of the left magnet is directed upright and that directions of other magnetization vectors of the magnets located from the right rotates clockwise by the angle of 45°C. In the FEM-model, if the magnets are present by their Ampere models, this correspond to alteration of the current densities of the x-layers in proportion to cosine of the angle between the magnetization direction and the x-axis and in the y-layers in proportion to sine of that angle.

Modeling separately fields produced by x- and y-current layers (fig. 5) and comparing the normal flux-density distributions along the straight contours $\grave{A}_1 B_1$ and $\grave{A}_2 B_2$ we can notice that at the low contour $\grave{A}_2 B_2$ flux-density normal components add summarizing and intensify the resultant field whereas at the upper contour $\grave{A}_1 B_1$ flux-density normal components opposite direction and the resultant field is mitigated.

Other applications of Halbach arrays in PMEM are well known and widely described in the literature: (Halbach, Design of permanent multipole magnets with oriented rare-earth cobalt material, 1980), (Halbach, Physical and optical properties of rare-earth cobalt magnets, 1981), (Halbach, Application of permanent magnets in accelerators and electron storage rings, 1985), (Zhu & Howe, Halbach permanent magnet machines and applications: A review., 2001), (Attalah & Howe, 1998), (Sotelo, Ferreira, & Andrade Jr, 2005), (Zhu, et al., 2003), (Jang, Leong, Ryu, & Choi, 2001).

As it was noticed, analytical expressions derived above refer to magnetic systems that have no soft magnetic elements on the inductor (field exiting) part. Nevertheless, if such elements are present, in the case of tangentially magnetized PMs they can be called magnetic flux concentrators, recommendations for the choice of reasonable dimensions can be obtained using the *FEM* models.

Numerical experiments

Finite element model presents a system consisting of permanent magnets and soft-magnetic-material flux concentrators located at a distance of an air gap α from ferromagnetic surface. Magnetic flux density distribution in the air gap was calculated in magnetostatic finite element model and expanded into a Fourier series. Air-gap length is accepted as the base dimension. The magnetic properties of the ferromagnetic core and flux concentrators material were defined by a real magnetization curve of electrical steel. Ferromagnetic parts are slightly saturated. The finite-element model, materials assigned and boundary conditions are shown on Fig. 6.

The examples of the research of an optimal ratio of the permanent magnets width to the pole pitch τ_m/τ in the design of permanent magnet linear machines with tangential magnetization are known(Bianchi, Bolognani, Corte, & Tonel, 2003).

As a result of the first experiment on the model described above dependences of the amplitude of the first harmonic of the magnetic flux density along the air gap at different ratios of the width of the permanent magnets to the pole pitch were plot. The calculation was performed for $\alpha = 1...2$ mm, $h_m/\alpha = 1...10$, $\tau/\alpha = 8...24$ and a given properties of the permanent magnets NdFeB 38 SH ($H_c = 900$ kA/m, $B_r = 1.22$ T, $\mu_r = 1.0787$). Plots of this dependences for $\alpha = 1$ mm$\tau/\alpha = 6$ are shown at Fig. 7.

The maximum of flux density $B_{\alpha 1m} = f(\tau_m/\tau)$ is achieved for all h_m/α and all ô/ä for the width of the magnet $\tau_m = [0{,}7 \div 0{,}8] \cdot \tau$. It can be seen that smaller values of maximum flux density $B_{\tau 1m}$ are typical for larger values of the relative length of the pole pitch τ_m/α.

In the next experiment the dependence of the first harmonic magnitude of the flux density along the middle line of the air gap on the ratio of the length of the pole pitch and the length of the air gap τ/α for different values of the ratio of the magnet height to the length of the gap h_m/α was obtained.

The geometrical dimensions of the model were changed in the following range: $\alpha = 1...2$ mm, $h_m/\alpha = 1...10$, $\tau/\alpha = 1...40$. The ratio of the magnet width to the pole pitch remained $\tau_m/\tau = 0{,}7$ for all τ/α. The plots of $B_{\alpha 1m} = f(\tau/\alpha, h_m/\alpha)$ obtained for the same properties of permanent magnets as in the first experiment are depicted at Fig.8.

By means of numerical simulations it was confirmed that the obtained dependencies can be used for the magnets with another magnetic properties. In this case the calculated values of the first harmonic amplitude of flux density in the gap should be related to the residual flux density of the magnet $B_{\alpha 1m}/B_r$.

The obtained dependences can be used

to find the optimal length of the pole pitch and permanent magnets height providing the desired flux density in the air gap. The plots of the permanent magnets relative height vs relative length of the pole pitch $h_m/\alpha = f(\tau/\alpha)$ for $B_{\alpha 1m} = const$ are shown at Fig. 9.

It can be seen that both plots at Fig. 8 and Fig. 9 have a distinct extremum and change smoothly enough to the right of the extremum. At the initial design stage it allows to select the basic dimensions of a linear machine which are close to optimal with respect to the minimum mass of the permanent magnets.

CONCLUSION

The analytical expressions for the normal component of the magnetic flux density calculation on the surface of a smooth ferromagnetic core created by a system of permanent magnets in the absence of the soft magnetic part was obtained. The formulas were tested on finite element models.

As a result of a series of numerical experiments the dependence of the first harmonic of the magnetic flux density along the middle line of the air gap on the ratio of the pole pitch length and the length of the air gap τ/α and for different values of the ratio of the magnet height to the length of the gap h_m/α was obtained. The results of the experiments may be used for selection of the optimal size of the permanent magnets and the pole pitch length at the initial design stage of a linear machine with longitudinally magnetized permanent magnets.

REFERENCES

1. Amara, Y., & Barakat, G. Analytical Modeling of Magnetic Field in Surface mounted Permanent-Magnet Tubular Linear Machines. *Ieee transactions on magnetics,* 2010; **46**(11).

2. Attalah, K., & Howe, D. The application of halbach cylinders to brushless AC servo motors. *IEEE transactions on magnetics,* 1998; **34**(4), 2060-2062.

3. Bianchi, N., Bolognani, S., Corte, D. D., & Tonel, F. Tubular Linear Permanent Magnet Motors: An overall comparison. *IEEE transactions on industry applications,* 2003; **9**(2).

4. Chu, W., & Zhu, Z. On-Load Cogging Torque Calculation in Permanent Magnet Machines. *IEEE transactions on magnetics,* 2013; **49**(6).

5. Gysen, B., Meesen, K., Paulides, J., & Lomonova, E. General formulation of the electromagnetic field distribution in machines and devices using Fourier analysis. *IEEE transactions on magnetics,* 2010; **45**(6); 39-52.

6. Halbach, K. Design of permanent multipole magnets with oriented rare-earth cobalt material. *Nuclear Instruments and Methods,* 1980; **169**: 1-10. doi:10.1016/0029-554X(80)90094-4

7. Halbach, K. Physical and optical properties of rare-earth cobalt magnets. *Nuclear Instruments and Methods,* 1981; **187**: 109-117. doi:10.1016/0029-554X(81)90477-8

8. Halbach, K. Application of permanent magnets in accelerators and electron storage rings. *Journal Applied Physics,* 1985; **57**: 3605-3608.

9. Hoburg, J. F. Modeling maglev passenger compartment static magnetic fields from linear halback permanent-magnet arrays. *IEEE transactions on magnetics,* 2004; **40**(1), 59-64.

10. Ivanov-Smolenskii, A., & Abramkin, Y. *Application of conformal mapping for electromagnetic analysis of electric machines (in Russian).* Moscow: MPEI Publishing house 1980.

11. Ivanov-Smolenskii, A., & Abramkin, Y. V. *Application of conformal mapping for electromagnetic analysis of electric machines: Analytical methods (in Russian).* 1970; Moscow: Energiya.

12. Jang, S.-M., Leong, S.-S., Ryu, D.-W., & Choi, S.-K. Design and analysis of high-speed slotless PM machine with Halbach array. *IEEE transactions on magnetics,* 2001; **37**(4): 2827-2830.

13. Jang, S.-M., You, D.-J., Ko, K.-K., & Choi, S.-K. Desing and experimental evaluation of synchronous machine without iron loss using double-sided Halbach magnetized PM rotor in high power FESS. *IEEE transactions on magnetics,* 2008; **44**(11): 4337-4340.

14. Krop, D., Lomonova, E., & Vandenpit, A. Application of Schwartz-Cristoffel mapping to permanent magnet linear motor analysis. *IEEE transactions on magnetics,* 2008; **44**(3).

15. Li, W., Chau, K., Liu, C., Gao, S., & Wu, D. Analysis of tooth-tip leakage in surface-mounted permanent magnet linear vernier machines. *IEEE transactions on magnetics,* 2013; **49**(7): 3949-3952.

16. Overboom, T., Smeets, J., Jansen, J., & Lomonova, E. Topology comparision for a magnetically suspended ceiling actuator. *Proc. IEEE International Electrical Machines and Drives Conference (IEMDC)*, 2011; (pp. 296-301).

17. Overboom, T., Smeets, J., Jansen, J., & Lomonova, E. Semianalytical calculation of the torque in a linear permanent-magnet motor with finite yoke length. *IEEE transactions on magnetics,* 2012; **48**(11).

18. Sotelo, G., Ferreira, A., & Andrade Jr, R. d. Halbach array superconducting magnetic bearing for flywheel energy storage system. *IEEE transactions appl. supercond.,* 2005; **15**(2), 2253-2256.

19. Wu, L., Zhu, Z., Staton, D., Popesku, M., & Hawkins, D. Analytical modeling and analysis of open-circuit magnet loss in surface-mounted permanent-magnet machines. *IEEE transactions on magnetics,* 2012; **48**(3), 1234-1247.

20. Zarko, D., Ban, D., & Lipo, T. A. Analytical Solution for Cogging Torque in Surface Permanent-Magnet Motor Using COnformal Mapping. *IEEE transactions on magnetics,* 2008; **44**(1).

21. Zhu, Z., & Howe, D. Halbach permanent magnet machines and applications: A review. *IEEE Proc. Electrical Power Applications,* 2001; **148**(4): 299-308.

22. Zhu, Z., Xia, Z., Shi, Y., Howe, D., Pride, A., & Chen, X. Performance of Halbach magnetized brushless AC motors. *IEEE transactions on magnetics,* 2003; **39**(5): 2992-2994.